Materials Today Bio 27 (2024) 101144

Contents lists available at ScienceDirect

Materials Today Bio

journal homepage: www.journals.elsevier.com/materials-today-bio

An intratumor bacteria-targeted DNA nanocarrier for multifaceted tumor microenvironment intervention

Yibiao Wang [a,1], Xiaomei Fu [a,1], Yang Zhu [a], Mingjing Lin [a], Renduan Cai [a,**], Yang Zhu [b,***], Tiantian Wu [c,*]

[a] Department of Neurosurgery/Department of Pediatrics/Department of Neonatal, Hainan General Hospital/Hainan Affiliated Hospital of Hainan Medical University, Hainan Medical University, Haikou, 570311, China
[b] Fujian Provincial Institutes of Brain Disorders and Brain Sciences/Department of Neurosurgery, Neurosurgery Research Institute, The First Affiliated Hospital, Fujian Medical University, Fuzhou, 350005, Fujian, China
[c] School of Pharmacy, Hainan Medical University, Haikou, China

ARTICLE INFO

Keywords:
DNA self-assembly
Intratumor bacteria
Tumor microenvironment
Berberine
Targeted delivery

ABSTRACT

Intratumor bacteria, which are involved with complex tumor development mechanisms, can compromise the therapeutic efficiencies of cancer chemotherapeutics. Therefore, the development of anti-tumor agents targeting intratumor bacteria is crucial in overcoming the drug inactivation induced by bacteria colonization. In this study, a double-bundle DNA tetrahedron-based nanocarrier is developed for intratumor bacteria-targeted berberine (Ber) delivery. The combination of aptamer modification and high drug loading efficacy endow the DNA nanocarrier TA@B with enhanced delivery performance in anti-tumor therapy without obvious systemic toxicity. The loaded natural isoquinoline alkaloid Ber exhibits enhanced antimicrobial, anticancer, and immune microenvironment regulation effects, ultimately leading to efficient inhibition of tumor proliferation. This intratumor bacteria-targeted DNA nanoplatform provides a promising strategy in intervening the bacteria-related microenvironment and facilitating tumor therapy.

1. Introduction

Tumor-resident microbiota is an emerging component that has been documented for a variety of cancer-related biological functions and mechanisms [1–3]. Recent evidence is gradually validating that bacteria are integral components of the tumor across a wide range of cancer types [3,4]. Intratumor bacteria promote tumor metastatic colonization and influence the responses of tumor cells to immunotherapy in various cancers. Research has shown that depleting intratumor bacteria leads to a significant reduction in tumor metastasis [1,3,5]. The presence of colonized bacteria as environmental factors can alter the metabolism, growth pattern, and function of neoplastic cells, leading to the reshaping of the tumor microenvironment during the process of tumor formation [6]. Given the close association between treatment effects and the tumor microenvironment, as well as the immune microenvironment, the impact of bacteria present within tumors on tumor initiation, promotion, and progression is complex [4,7]. Additionally, the presence of intratumor bacteria can compromise the therapeutic efficacy in chemotherapy. First-line chemotherapeutic, such as gemcitabine, are observed to be counteracted and metabolized into inactivated form by intratumor bacteria [3,8]. The increasing drug inactivation gradually leads to cancer drug resistance and finally posing challenges to clinical cancer treatment. Overall, intratumor bacteria play a pivotal role in unraveling the mechanisms of tumor resistance and serve as a research target for the development of anticancer drugs.

To overcome the tumor metastatic promotion and drug inactivation induced by bacteria colonization, the development of strategy combined antitumor treatment with specific sterilization is expected to enhance the therapeutic effect. Broad-spectrum antibiotics are commonly used as the first-line anti-infection drugs in antibacterial treatment [9,10]. However, indiscriminate systemic bacteria killing compromises body microbiome diversity and could impair the efficacy of immune-related

* Corresponding author.
** Corresponding author.
*** Corresponding author.
E-mail address: wutiantian@hainmc.edu.cn (T. Wu).
[1] These authors equally contributed to this work.

https://doi.org/10.1016/j.mtbio.2024.101144
Received 2 April 2024; Received in revised form 26 June 2024; Accepted 1 July 2024
Available online 3 July 2024

tumor inhibition [11–13]. In addition, the complex barrier of tumor microenvironment restricts the permeation of antibiotics into the tumor. High-dose medication and repeat exposures to antibiotics can also lead to variety of adverse effects [14,15]. Therefore, selective targeting of intratumor bacteria associated with cancer chemotherapeutics holds the potential to effectively inhibit the growth of the intratumor bacteria and alleviate bacterium-induced drug inactivation [16,17].

Nanoparticle-based drug delivery carriers possess significant advantages in enhancing drug accumulation and improving therapeutic efficacy [10,18–20]. Precisely combined therapy can also be achieved by targeted ligand modification on the drug carriers. DNA nanostructures, which have demonstrated high drug-loading capability and superior biocompatibility, have been utilized to deliver therapeutic drugs to targeted regions for various diseases treatment [21–24]. Functional groups, including targeted ligands, signal probes, catalytic groups, and drug molecules, can be precisely organized on DNA nanocarriers to generate vital properties for targeted accumulation and controlled release [19,25]. The loading strategy for drugs and functional ligands based on noncovalent binding endow DNA self-assembly nanocarrier with high loading efficiency and simplified synthesis procedure. Avoiding complex chemical synthesis, the facile preparation process effectively enhances the therapeutic effect of antibiotics. While outstanding performance has been achieved in sterilization, the development of DNA nanocarrier has not been fully explored for achieving a synergistic intervention effect of the loading functional components. Based on tailored properties above, we hypothesized that agents with antibacterial activity could be efficiently loaded in the precisely self-assembled DNA nanostructures and effect enhanced tumor microenvironment regulatory functions by targeted delivery.

Berberine (Ber), as one of the most used natural isoquinoline alkaloid worldwide, is a potent alkaloid with considerable pharmacological activities, including antimicrobial, anticancer, and anti-inflammatory effects [26–28]. In this study, we present a universal strategy for intratumor bacteria-targeted Ber delivery (Scheme 1). A bacteria-specific double-bundle DNA tetrahedron was firstly developed for recognizing and binding with intratumor bacteria. Through site-specific hybridization of multiple bacteria-specific aptamers, the DNA tetrahedron with Aptamer (TA) accumulates in tumor through enhanced permeability retention effect, penetrates into the tissue, and binds with bacteria. The ternary function agent Ber was efficiently loaded into the TA through intercalation-based noncovalent binding with DNA duplex. This drug-loading strategy achieved high delivery performance without the need for complicated chemical reactions and purification processes. The enhanced tumor cell inhibition, antibacterial activity, and immune regulation effects of TA@B co-ordinately regulate tumor microenvironment and significantly inhibit tumor growth. This rationally designed nanocarrier, namely TA@B, with controllable size and shape exhibits excellent targetability and effective antitumor efficacy without detectable systemic side effects *in vivo*. Our study demonstrated the first example of intratumor bacteria-targeted DNA platform for multifaceted tumor microenvironment intervention-based cancer therapy.

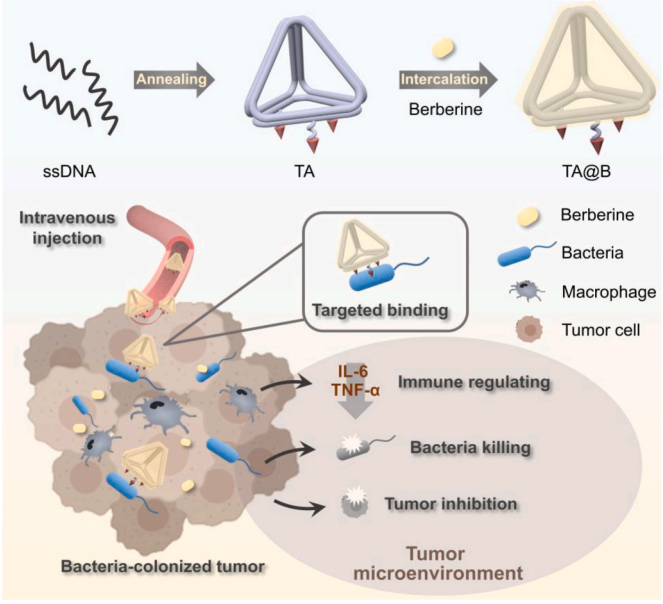

Scheme 1. A schematic representation of the DNA tetrahedron-based intratumor bacteria-targeted DNA nanocarrier for multifaceted tumor microenvironment intervention-based cancer therapy. The loaded Ber exhibits enhanced antimicrobial, anticancer, and immune regulation effects, ultimately leading to efficient inhibition of tumor proliferation.

2. Experimental section

2.1. Materials

Chemicals and solvents were obtained commercially and used without further purification. Millipore water was used to prepare all aqueous solutions. All DNA oligonucleotides used in this study were purchased from Huzhou Hippo Biotechnology Co., Ltd. Dimethyl sulfoxide, LPS, and crystal violet were purchased from Aladdin (Shanghai). Live & Dead Bacterial Staining Kit (cat# 40274ES60), MolPure® Bacterial RNA Kit (cat#18806), and Hifair® III One Step RT-qPCR SYBR Green Kit (cat#11143ES70) were purchased from Yeasen, Shanghai, China. TUNEL staining kit was purchased from Solarbio kit (Beijing, China). The bacteria strain *Escherichia coli* was obtained from BeNa Culture Collection (Beijing, China). The bacteria strain was maintained in LB broth supplemented at 37 °C with shaking (225 rpm). 4T1 cell was purchased from the American Type Culture Collection. The 4T1 cells were maintained in DMEM supplemented with 10 % FBS and penicillin/streptomycin in a humidified atmosphere containing 5 % CO_2 at 37 °C.

2.2. Construction and characterization of TA@B

DNA tetrahedron used in this work is modified from previous reports from Ding's research [29]. DNA sequences used in this study for DNA tetrahedron assembly are shown inTable S1. Table S1. The *E. coil*-specific aptamer (CATATCCGCGTCGCTGCGCTCAGACCCACCACCACGCACC) was stretched from the hybridization sequence. Concentrations of purified oligonucleotides were determined by measuring UV absorbance at 260 nm. The purified DNA strands were mixed at the same molar ratio in a 1 × TAE/Mg^{2+} buffer (40 mM Tris, 20 mM acetic acid, 2 mM EDTA, and 12.5 mM magnesium acetate, pH = 8.3) with the final concentration of 1 μM. The aforementioned assembly solutions were kept at 95 °C for 3–5 min and then cooled down from 95 to 25 °C over 24 h. For the preparation of TA@B, Ber was pre-dispersed in DMSO with a concentration of 5 mM. Then, the TA was added with different ratios of Ber from 1:1 to 1:4 (DNA base pair: Ber) and cultured at 25 °C for 3 h. After the loading process, the TA@B was purified by an Amicon stirred cell (UFSC05001) equipped with 5 kDa ultrafiltration disc under nitrogen pressure to filter the samples under continuous stirring to avoid the possible aggregation by high local concentration. The unloaded Ber was quantified by measuring UV absorption at 325 nm. The drug loading efficiency (DLE) was calculated according to the following equations:

$$\text{DLE } \% = \frac{\text{Ber added} - \text{free Ber}}{\text{Ber added}} \times 100\%$$

The prepared samples were imaged with an Ht7800 TEM (Hitachi) and MultiMode 8 AFM (Bruker). Dynamic light scattering of DNA tetrahedron (50 nM) was performed on a Malvern Zetasizer Nano-ZS (Malvern Instruments, U.K.).

2.3. Evaluation of ber release

TA@B was separated into 1 mL of PBS (pH 6.0, pH 7.4, or pH 8.3) and sealed in a dialysis bag (3 KDa). The dialysis bag was immersed in 10 mL of PBS with the corresponding pH and then incubated with continuous shaking at 37 °C. At the predesigned time intervals, 1 mL of dialysate was collected from each sample, and 1 mL of the corresponding buffer was added to the remaining dialysate. The collected dialysate was analyzed using a UV spectrophotometer.

2.4. Bacterial binding analysis

Bacteria strand *E. coli* (gram-negative, BNCC336902) was utilized for performance study. For bacterial binding analysis, activated *E. coli* (1×10^8) was cultured with 100 μL of the Cy5-labeled DNA tetrahedron. The concentration of samples was based on Cy5 (1 μM). The mixture was incubated at 37 °C for 30 min. After culture, Bacteria were then collected by centrifuging (4000 rpm, 1 min) and washed with PBS for 3 times. Then, the bacteria were transferred to confocal dish and covered with a glass coverslip for laser scanning confocal microscopy (LSCM) imaging (Carl Zeiss, Germany).

In the bacteria-infection model, TA (1 μM Cy5) was pre-mixed with *E. coli* (1×10^8) for 5 min. Then, the mixture was added into the confocal dish with pre-adhesion 4T1 cell. After 0.5 h incubation, Calcein AM (10 μM) was added for 4T1 staining. The samples were washed with PBS. Then, the supernatant containing bacteria was transformed back to the confocal dish and imaged by CLSM.

2.5. Antimicrobial activity tests

The antimicrobial activity was tested on *E. coil*. Briefly, the bacterial suspensions (5×10^5 CFU/mL) were resuspended in the LB broth. Then the drugs were added and the drug concentration of different components was based on 1 mM Ber. After 12 h of incubation, the OD_{600} value was measured for relative bacterial viability analysis.

The bacteria after different treatments were centrifuged (4000 rpm, 5 min) and redispersed in 0.5 mL test buffer. Then, DMAO (Ex/Em = 503/530 nm) and EthD-III (Ex/Em = 530/620 nm) were added following the instructions of the Live & Dead Bacterial Staining Kit for staining. After incubation, bacteria cells were centrifuged, washed with PBS for 3 times, and observed by CLSM.

2.6. Cellular cytotoxicity assay

4T1 cells were seeded in 96-well plate with 5×10^3 cells per well and cultured overnight for cell adhesion. Then, the medium was replaced by 100 μL of OPTI-MEM medium containing drugs. The concentration of each sample was based on 1 mM Ber. For the bacteria-infected model, the *E. coli*-tumor cell mixture (5×10^3 4T1 cells with 1×10^5 *E. coli*) was treated with drugs based on 1 mM Ber. The cells were further incubated for 48 h at 37 °C. Then the medium with drugs was replaced by fresh culture medium containing Cell Counting Kit-8 (CCK8) solution. After the incubation of 0.5 h at 37 °C, the absorbance at 450 nm was measured using a Bio-Rad 680 microplate reader.

2.7. Quantitative RT-PCR assay

Total RNA was extracted by the MolPure® Bacterial RNA Kit following the instructions. Briefly, *E. coil* (1×10^8) treated with different drugs were harvested, washed with cold PBS, and retreated with RNA protect Buffer. The isolation of RNA was conducted on ice, followed by reverse transcription of the total RNA into cDNA. Subsequently, the quantitative real-time PCR analysis of the cDNA samples (100 ng) was performed using the RT-qPCR SYBR Green Kit. Primer sequences are shown inTable S2. Table S2. Quantitative real-time PCR was performed using the Multicolor Real-Time PCR Detection System (Bio-Rad, CA, USA).

2.8. In vitro immune regulation

To evaluate the anti-inflammatory efficiency, 3×10^5 RAW 264.7 cells were inoculated into 6-well plates overnight. The cells were then treated with lipopolysaccharide (LPS, 100 ng mL^{-1}) for 12 h to induce inflammation. Then the induced cells were incubated with PBS, Ber, and TA@B for 12 h. After the incubation, the TNF-α and IL-6 level was determined by an enzyme-linked immunosorbent assay (ELISA) kit.

2.9. Animals and tumor model-building

Female BALB/C mice (6 weeks) were obtained from Beijing Vital River Laboratory Animal Technology Co., Ltd. All animal-related procedures were approved by the Institutional Animal Care and Use Committee of Hainan Medical University with ethics approval (HYLL-2023-182). *E. coli*-infected 4T1 tumor model was constructed for *in vivo* antitumor suppression test. For 4T1 tumor model-building, 5×10^5 4T1 cells in 100 μL of PBS were subcutaneously injected. When the tumor volume reached 100 mm^3, *E. coil* (1×10^6, 20 μL) was injected intratumorally for *in vivo* experiments.

2.10. Hemolysis assay

Red blood cells extracted from healthy mice were centrifuged, washed with cold PBS, and appropriately diluted to prepare a cell suspension. The PBS, Ber, TA@B, and H_2O (as positive control) were added into the red blood cell suspension and the mixture was incubated at 37 °C for 3 h. Then, the absorbance value of the supernatant obtained by centrifugation was measured at 541 nm.

The calculation formula for the relative hemolysis rate was as follows:

$$\text{Relative hemolysis} = \frac{OD(\text{Drug}) - OD(\text{PBS})}{OD(\text{H2O}) - OD(\text{PBS})} \times 100\%$$

2.11. Statistical analysis

Data represent the mean ± s.d. from indicated independent replicates. Statistical analysis was conducted using GraphPad Prism. For comparisons between two groups, means were compared using the unpaired two-tailed Student's t-test. A value of $P < 0.05$ was considered statistically significant.

3. Results and discussion

3.1. Construction and characterization of the TA@B

For intratumor bacteria-targeted drug delivery, we aimed to construct a self-assembly double-bundle DNA tetrahedron-based drug carrier with targeted ligand modification for Ber delivery. The detail sequences for DNA tetrahedron synthesis are shown in Table S1. Table S1 in the supporting information. After a programmed annealing process, the aptamer-modified TA was acquired with the concentration of 1 μM. Then, we optimized the drug loading efficacy at different DNA duplex/Ber molecular ratios (1:0.5, 1:1, 1:2, and 1:4). After obtaining optimized loading parameters, the Ber-loaded DNA tetrahedron was characterized with dynamic light scattering (DLS), atomic force microscope (AFM), and transmission electron microscope (TEM) as shown in Fig. 1A–D. As researchers had investigated that the flavonoids-based isoquinoline alkaloid berberine reacts with DNA mainly through intercalation and electrostatic interaction [30,31], in our study, the Ber loading procedure was conducted following the loading process we previously reported [19,29]. UV absorption analysis at 325 nm revealed that the feed ratio of 1:4 and 3 h incubation had the highest drug-loading efficiency (DLE) of 45.6 % (Fig. 1E). Based on the results of morphology characterization, monodisperse nanostructures were observed by AFM

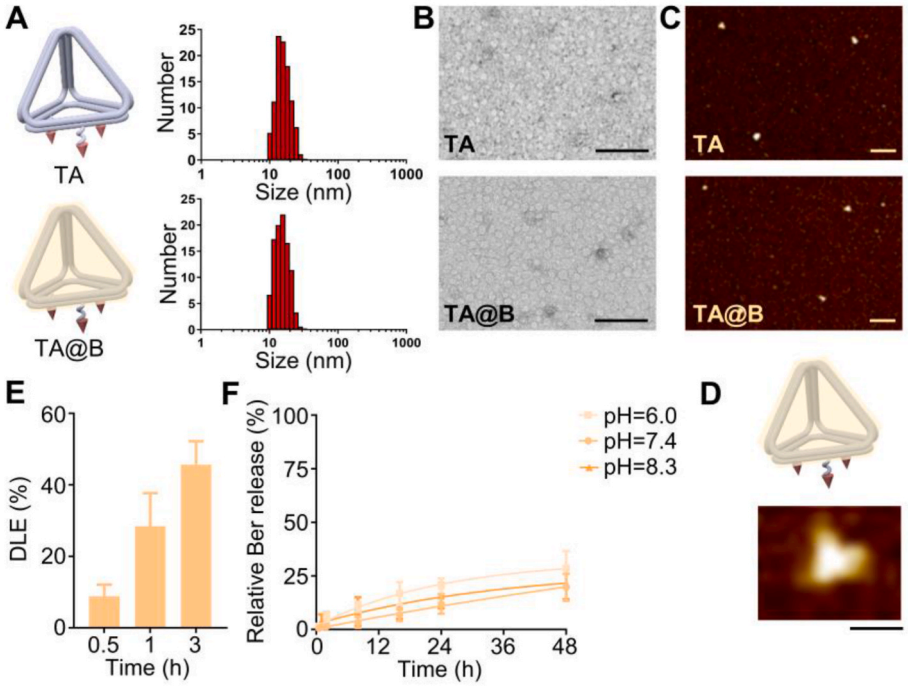

Fig. 1. Preparation and characterization of the DNA tetrahedron-based drug nanocarrier. (A) Hydrodynamic diameters of the TA and TA@B measured by dynamic light scattering. (B) TEM images of TA and TA@B. Scale bar: 50 nm. (C) AFM images of TA and TA@B. Scale bar: 50 nm. (D) High-resolution AFM images of the TA@B. Scale bar: 10 nm. (E) Drug loading efficiency analysis of Ber-loaded DNA tetrahedron TA@B after different time of incubation. (F) Time-dependent Ber release curve of TA@B at different pH.

and TEM. A clear tetrahedral-like shape was characterized by high resolution AFM imaging. No aggregation was found during the drug-loading procedure. The hydrodynamic particle size of TA@B measured by DLS was 14.5 ± 0.7 nm, which was slightly larger than the unloaded TA of 13.2 ± 0.6 nm. The loading of Ber slightly increased the diameters of the DNA tetrahedron. Ber with photosensitivity is sensitive to drug-loading operations. The noncovalent binding of Ber with DNA duplex is a favorable strategy for Ber loading effectively.

Subsequently, the drug release efficacy of Ber and stability in serum were investigated to evaluate the delivery performance. The drug release behaviour was investigated in different pH mimicking different physiological conditions in blood, tumor acidic, and inflammatory alkaline conditions, respectively. As shown in Fig. 1F, TA@B exhibited a slow and sustained release in a time-dependent manner and achieved a reluctant release of 25 % within 48 h. The stability was tested in DMEM (with 10 % FBS) at 37 °C for different time intervals. After a 36-h incubation, over 63 % of the DNA structure remained intact (Fig. S1–2). The stability and release performance of the drug are critical for nanocarrier in disease treatment. The Ber-loaded nanocarrier would be favorable for Ber delivery and treatment.

3.2. *In vitro antibacterial activity evaluation*

Escherichia coli (*E. coli*) and biofilm have been associated with the promotion of colorectal cancer development and was found to be abundant in the breast cancer tissue microenvironment [32–34]. We employed *E. coli* to verify the antibacterial performance of the TA@B. Targeted recognition and specific binding are crucial for the therapeutic effect of drug carriers. To investigate the cellular binding efficiency, we used fluorescent dyes FITC-labeled DNA strand to prepare Td (-Apt) without aptamer modification and TA for confocal imaging analysis. TA with 3 aptamers stretched out showed a greater affinity to bacterial cells compared to Td (Fig. 2A). As shown in Fig. 2B, TA also showed a strong binding selectivity with bacteria in the co-incubation system involving tumor cells (4T1). These results indicate that the targeted Ber nanocarrier holds the potential for selectivity against bacteria at the tumor site.

In anti-infection, Ber showed significant antimicrobial activity against several microbes through inhibiting the bacteria cell division. In this study, the inhibitory effects of different drugs on *E. coli* were surveyed via a series of evaluations. After treated with Ber for 12 h with the concentration of 1 mM, broadly apoptosis occurred and the growth of *E. coli* was inhibited. We stained *E. coli* with DMAO (Ex/Em = 503/530 nm) and EthD-III (Ex/Em = 530/620 nm), followed by imaging using a confocal laser scanning microscope (CLSM) according to the instructions of the Live & Dead Bacterial Staining Kit (Fig. S3). As shown in CLSM images, PBS-treated cells were stained by simply green fluorescence, while red fluorescence occurred in the free Ber and TA@B group. In bacterial viability analysis, the treatment of Ber-loaded nanocarrier with the same concentration of drugs exhibited enhanced elimination effect, especially with the guidance of the *E. coli*-targeted aptamer (Fig. 2C–D). The TA@B exhibited an excellent antibacterial rate up to 63.1 %, which is significantly higher than free Ber. To further determine the antibacterial effect, we verified sustained inhibition of *E. coli* by preparing a drug-containing Luria-Bertani (LB) agar dish (Fig. S4). The TA@B displayed a long-term inhibition effect over 24 h. In micromorphology analysis performed by TEM imaging, the morphology of *E. coli* appeared irregular and collapsed after treated with Ber. The Td@B(-Apt) treatment break the structure of the bacteria and in contrast, TA@B completely destroyed the bacterial cell. Taken together, the targeted Ber nanocarrier exhibits exceptional antibacterial activity *in vitro*.

3.3. *Cell proliferation inhibition analysis*

Ber has been broadly used in cancer therapy as an active agent to inhibit cancer cell proliferation and induce cell apoptosis [26,30,35]. We at first tested apoptosis induced by different drugs on 4T1 cells to verify their effects on cell proliferation inhibition. Based on results of cell apoptosis imaging, at the indicated drug concentrations based on 1 mM Ber, free Ber induced broadly early apoptosis (Annexin V-FITC

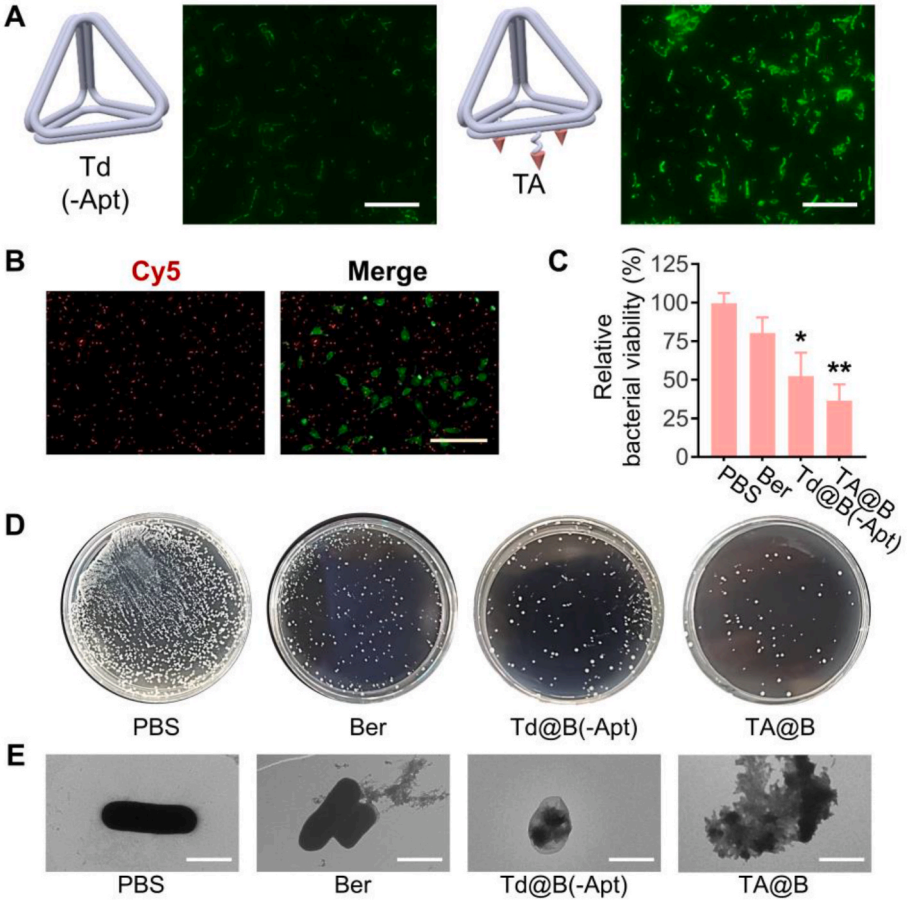

Fig. 2. *In vitro* antibacterial performance analysis. (A) Confocal images of FITC-labeled Td (-Apt) and FITC-labeled TA on *E. coil*. Scale bar: 10 μM. (B) Confocal images of 4T1 cells co-cultured with *E. coil*. The cell mixture was treated with Cy5-TA for 0.5 h at 37 °C. DNA tetrahedron was labeled with Cy5, red; 4T1 cell was stained with Calcein AM, green. (C) Relative bacterial viability after the treatment of TA, Ber, and TA@B. The drug concentration is based on 1 mM Ber. (D) Photographs of the *E. coil* colonies from different treatment groups. (E) Micromorphologies of medicated bacteria. Scale bar: 1 μm. (*P < 0.05, **P < 0.01).

positive, green) after 12 h of the treatment, whereas TA@B remarkably exacerbated early apoptosis to necrosis (Annexin V-FITC positive/PI positive, green/red) of 4T1 cells (Fig. 3A). Apoptosis-related gene regulation was measured by quantitative RT-PCR (Fig. 3B). The remarkable downregulation of the Bcl-2 and significant upregulation of the Bax and cleaved caspase-3 (CC3) were observed. Results of the same trend in cell viability analysis were obtained by cell counting kit-8 assay. As shown in Fig. 3C, TA@B exhibited higher anticancer efficacy than free Ber after 48 h of incubation. The cell viability test was also applied in the *E. coli*-infected tumor cell model. In order to avoid imprecision measurement caused by excessive proliferation of bacteria, we take 24 h culture as proliferation test condition. As shown in Fig. 3D and S5, TA@B hold excellent anticancer ability to *E. coli*-infected cells as excepted (43.9 % inhibition). In addition to outstanding bactericidal capabilities, cytocompatibility is also essential for nanomaterials in biomedical applications. It is worth mentioning in cytotoxicity tests that the biocompatible TA did not exhibit any cytotoxicity at the indicated concentrations, indicating good biosafety of the DNA tetrahedron-based nanocarrier.

3.4. Immune regulation evaluation

The death of gram-negative bacteria can accelerate the release of LPS, which elicits the immune response with multiple cells involved [8]. The changes in tumor microenvironment caused by LPS have a complex and varied impact on tumor treatment. In addition to antimicrobial and antitumor activity, Ber can also counteract inflammatory conditions by suppressing the expression of inflammatory mediators such as TNF-α and IL-6. Thus, we evaluated proinflammatory cytokines in LPS-induced Raw 264.7 after different treatments by ELISA. As shown in Fig. 4A, the treatment of the Ber and TA@B treatment remarkably decreased the TNF-α and IL-6 level. The immunofluorescence images confirmed that after 12 h of TA@B treatment, the LPS-induced Raw 264.7 showed a noticeable expression of the anti-inflammatory factor TGF-β and IL-10 (Fig. 4B). Taken together, the TA@B inhibited the bacteria-related tumor immune response, restoring the balance in the tumor microenvironment disrupted by bacterial fragmentation.

3.5. In vivo anticancer therapy of TA@B

Encouraged by the excellent *in vitro* performances of the TA@B, we next proceeded to study the *in vivo* anticancer efficacy. The combination effect including antibacterial activity, tumor cell inhibition, and immune regulation of the loaded Ber, as illustrated in Fig. 5A, are expected to achieve enhanced tumor suppression effect through intratumor bacteria-targeted delivery. The *in vivo* tumor suppression efficiency was assessed in an *E. coil*-infected 4T1 mouse tumor model. The infected tumor on BALB/c mouse model was treated with PBS, Ber, and TA@B (based on 1 mg Ber/kg body weight) by tail vein injection, respectively. The administration was conducted every other day for 3 treatments on Day 0, Day 2, and Day 4. The tumors in the PBS control group exhibited rapid growth, reaching approximately nine times the initial tumor volume within 16 days. Compared with the control group, TA@B showed significant inhibition of tumor growth, which is in accordance with the

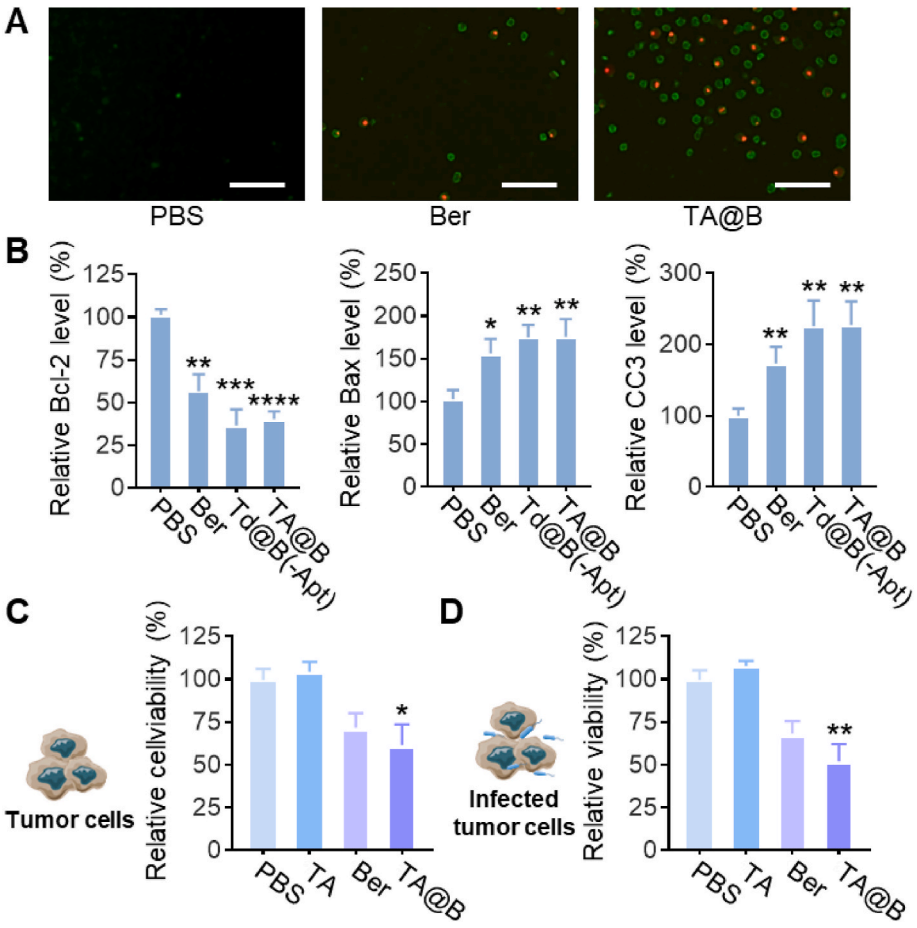

Fig. 3. *In vitro* anticancer performance analysis. (A) Cell apoptosis assay of different drugs (green fluorescence for Annexin V-FITC positive and red fluorescence for PI positive). Scale bars: 100 μm. (B) Quantitative RT-PCR analysis of relative mRNA level of apoptosis-related Bcl-2, Bax, and cleaved caspase-3 (CC3). (C) Cell viability of 4T1 cells after the indicated treatments at 37 °C for 48 h. (D) Cell viability of *E. coli*-tumor cell mixture after the indicated treatments at 37 °C for 24 h (*P < 0.05, **P < 0.01).

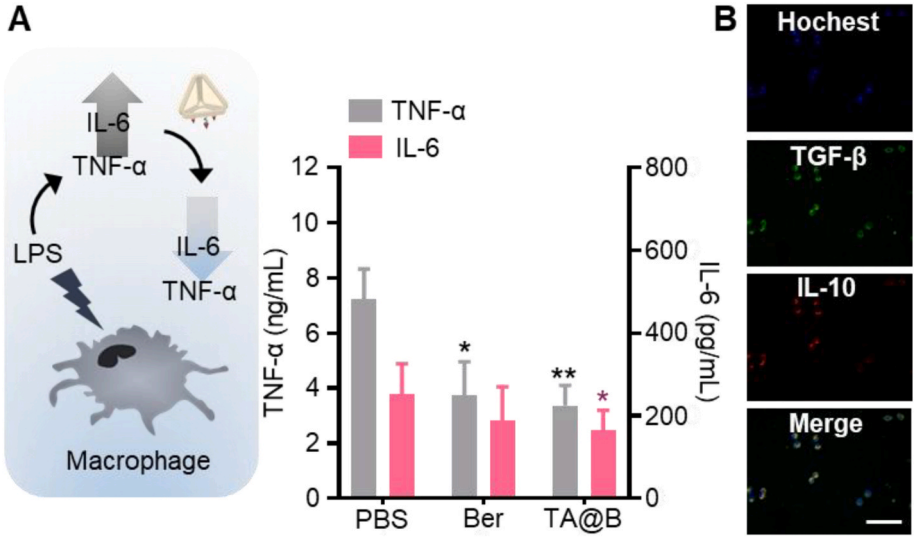

Fig. 4. *In vitro* immune regulation performance. (A) TNF-α and IL-6 expression in LPS-induced Raw 264.7 detected by ELISA kits. (B) Immunofluorescence images of LPS-induced Raw 264.7 after the treatment of TA@B (green fluorescence for TGF-β positive and red fluorescence for IL-10 positive). Scale bars: 10 μm. (*P < 0.05, **P < 0.01).

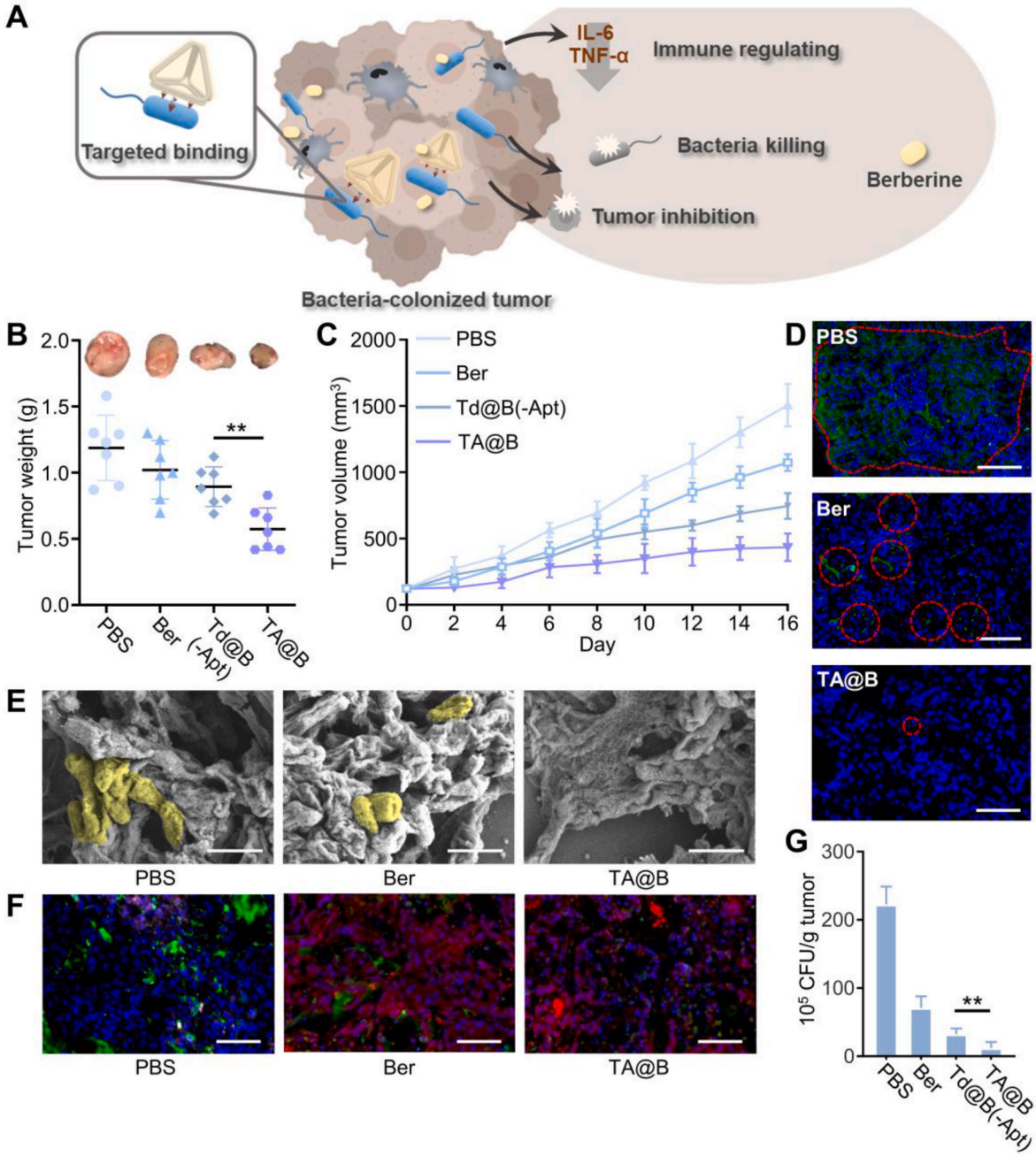

Fig. 5. *In vivo* antitumor performance of the Ber-loaded nanocarrier. (A) Illustration of the intratumor bacteria-targeted DNA nanocarrier for multifaceted tumor microenvironment intervention-based cancer therapy. (B) Weight of tumor in bacteria-infected tumor model. (dosage: 1 mg Ber/kg body, n = 8). (C) Growth curves of the *E. coil*-infected 4T1 tumors under different treatments. (D) Active oxygen quantitative imaging of tumor (green fluorescence for ROS). Blue fluorescence signal represents nucleus stained by DAPI. Scale bar: 100 μm. The red circle indicate the ROS signal region. (E) SEM images of tumor after the treatment of PBS, Ber, and TA@B. Bacteria in tumor tissue were marked with yellow color in the images. Scale bar: 1 μm. (F) Images of immunofluorescence staining of tumor tissues after different treatments. The samples were conducted with TUNEL assays (red fluorescence) and merged with GFP-transfected *E. coil* signal (green fluorescence). Scale bar: 50 μm. (G) Counting of *E. coil* colonies in tumor. (**P < 0.01).

cytotoxicity analysis *in vitro*. As shown in Fig. 5B, the weight of the TA@B-treated tumor (0.57 g on average) was remarkably lower compared to the PBS control group (1.19 g on average). Results with similar trends were collected through measuring the tumor volume (Fig. 5C). Bacterial colonization typically triggers a high level of ROS as part of the immune response. Next, we analyzed the ROS level of the tumor after different treatments. As shown in Fig. 5D, the ROS level was apparently decreased after the treatment of TA@B, suggesting the excellent anti-infection and immunomodulatory effects of the targeted delivery of Ber. Then, we analyzed the intratumor bacteria through scanning electron microscopy (SEM) imaging (Fig. 5E). After treated with TA@B, barely no intact bacteria cell can be observed in the images. In addition, the *E. coil*-related LPS was also at a relatively low level under the action of TA@B(Fig. S6). The tumor tissues harvested from mice were also stained with TUNEL (Fig. 5F). The images exhibited that caused the most serious damage to the tumor tissues and TA@B induced the most severe cell apoptosis (red fluorescence). The counting of bacteria colonies in tumor homogenate is consistent with the results of the SEM imaging(Fig. 5G andS7). The intratumor GFP-transfected *E. coil* was thoroughly eliminated after the treatment of TA@B (Fig. 5E–F).

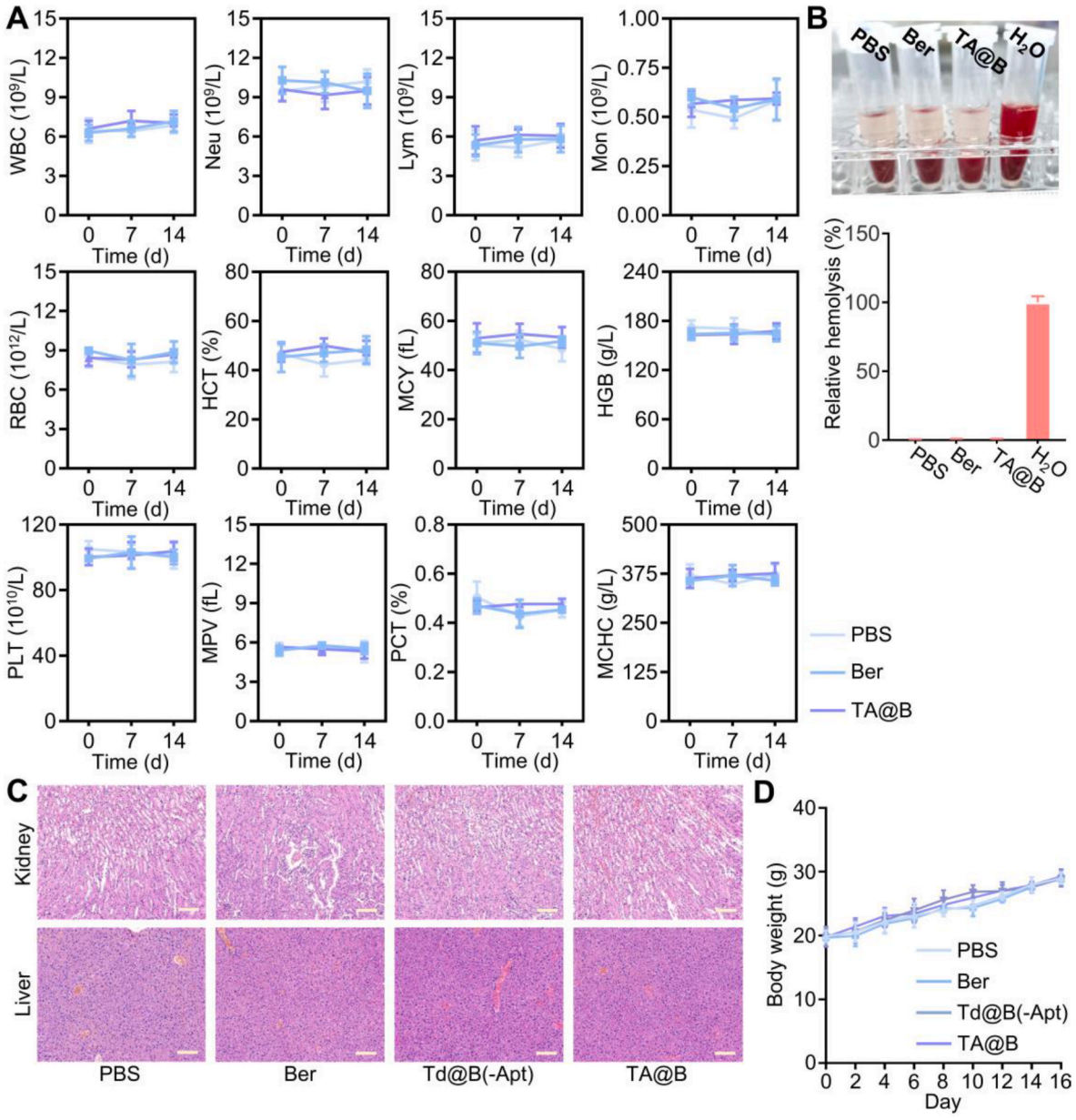

Fig. 6. *In vivo* biosafety analysis. (A) Routine blood examination of different treatments on days 0, 7, and 14. (B) Hemolysis analysis of Ber and TA@B. H_2O was utilized as the positive control. (C) H&E assays of the kidney and liver excised after different treatments. Scale bar: 50 μm. (D) Body weights of mice measured during the treatment.

Moreover, the level of inflammatory factors (TNF-α and IL-6) expressed in tumor tissue has been effectively reduced under the treatment (Fig. S8). Compared with free Ber, the strategy of targeted delivery of Ber demonstrated a significantly improved bacterial inhibition effect. The above results suggested that the DNA tetrahedron-based targeted nanocarrier hold exceptional therapeutic effects *in vitro*.

3.6. *In vivo* biosafety of TA@B

We further evaluated the *in vivo* biosafety of the DNA nanostructure-based nanocarriers. As shown in Fig. 6A, results of routine blood and biochemistry examinations indicated no significant changes in blood indices during the treatment. In hemolysis analysis, all treatment groups were with clear and transparent supernatant (Fig. 6B). The hemolysis rates in the Ber and TA@B treatment groups were below 1 %, suggesting that the DNA-based drug delivery platform did not cause hemolysis. In order to explore whether TA@B made damage to main organs of mice, after the treatment, H&E staining was utilized to observe the pathologic changes of the kidney and liver of mice in each group. Biodistribution analysis indicates high enrichment of the TA@B on bacteria-infected tumor(Fig. S9). As shown in Fig. 6C, had no discernible impact on the kidney and liver. In addition, the body weight of mice during the treatment were similar and steadily increased, providing strong evidence for the biosafety of the DNA nanoplatform (Fig. 6D).

4. Conclusions

In this study, an innovative DNA tetrahedron-based nanocarrier was fabricated for intratumor bacteria-targeted drug delivery and treating *E. coli*-infected cancer. The fabricated TA@B demonstrated excellent loading and delivery performance of Ber, effectively enhancing the antibacterial, anti-tumor, and immune regulation effects in the tumor microenvironment. This multifunctional Ber nanocarrier exhibited unique advantages for microenvironment-related cancer therapy.

Firstly, the addressable double-bundle DNA tetrahedron enables the arrangement of anti-bacterial aptamers to achieve a targeting effect. Secondly, the biocompatible DNA nanocarrier is tailored for effectively Ber loading through non-covalent interaction with DNA duplex. Finally, the ternary effects of the TA@B can realize a combined therapy in bacteria-related microenvironment. After the treatment of TA@B, we observed a noticeable inhibition of tumor growth *in vivo*. This targeted Ber delivery nanocarrier has the potential to be developed into a versatile platform for intervening in the tumor microenvironment through multiple pathways. We believe this multifunctional DNA nanoplatform will open a new avenue for targeted chemotherapy and provide inspiration in the study of tumor microenvironment intervention.

CRediT authorship contribution statement

Yibiao Wang: Writing – original draft, Software, Resources, Methodology. **Xiaomei Fu:** Conceptualization. **Yang Zhu:** Project administration, Methodology, Investigation. **Mingjing Lin:** Resources, Project administration, Methodology, Investigation. **Renduan Cai:** Writing – original draft, Supervision, Project administration. **Yang Zhu:** Writing – review & editing, Writing – original draft, Supervision, Conceptualization. **Tiantian Wu:** Writing – review & editing, Writing – original draft, Supervision, Funding acquisition.

Declaration of competing interest

The authors declare that they have no known competing financial interests or personal relationships that could have appeared to influence the work reported in this paper.

Data availability

Data will be made available on request.

Acknowledgements

This work was supported by the National Natural Science Foundation of China (82202532) and Hainan Provincial Natural Science Foundation of China (NHXXRCXM202318). The authors are grateful to the support of instruments and facilities provided by Public Researchenter of Hainan Medical University.

Appendix A. Supplementary data

Supplementary data to this article can be found online at https://doi.org/10.1016/j.mtbio.2024.101144.

References

[1] A. Fu, B. Yao, T. Dong, Y. Chen, J. Yao, Y. Liu, H. Li, H. Bai, X. Liu, Y. Zhang, C. Wang, Y. Guo, N. Li, S. Cai, Tumor-resident intracellular microbiota promotes metastatic colonization in breast cancer, Cell 185 (8) (2022) 1356–1372.

[2] C.M. Dejea, P. Fathi, J.M. Craig, A. Boleij, R. Taddese, A.L. Geis, X. Wu, C. E. DeStefano Shields, E.M. Hechenbleikner, D.L. Huso, R.A. Anders, F. M. Giardiello, E.C. Wick, H. Wang, S. Wu, D.M. Pardoll, F. Housseau, C.L. Sears, Patients with familial adenomatous polyposis harbor colonic biofilms containing tumorigenic bacteria, Science 359 (6375) (2018) 592–597.

[3] L.T. Geller, M. Barzily-Rokni, T. Danino, O.H. Jonas, N. Shental, D. Nejman, N. Gavert, Y. Zwang, Z.A. Cooper, K. Shee, C.A. Thaiss, A. Reuben, J. Livny, R. Avraham, D.T. Frederick, M. Ligorio, K. Chatman, S.E. Johnston, C.M. Mosher, A. Brandis, G. Fuks, C. Gurbatri, V. Gopalakrishnan, M. Kim, M.W. Hurd, M. Katz, J. Fleming, A. Maitra, D.A. Smith, M. Skalak, J. Bu, M. Michaud, S.A. Trauger, I. Barshack, T. Golan, J. Sandbank, K.T. Flaherty, A. Mandinova, W.S. Garrett, S. P. Thayer, C.R. Ferrone, C. Huttenhower, S.N. Bhatia, D. Gevers, J.A. Wargo, T. R. Golub, R. Straussman, Potential role of intratumor bacteria in mediating tumor resistance to the chemotherapeutic drug gemcitabine, Science 357 (6356) (2017) 1156–1160.

[4] D. Nejman, I. Livyatan, G. Fuks, N. Gavert, Y. Zwang, L.T. Geller, A. Rotter-Maskowitz, R. Weiser, G. Mallel, E. Gigi, A. Meltser, G.M. Douglas, I. Kamer, V. Gopalakrishnan, T. Dadosh, S. Levin-Zaidman, S. Avnet, T. Atlan, Z.A. Cooper, R. Arora, A.P. Cogdill, M.A.W. Khan, G. Ologun, Y. Bussi, A. Weinberger, M. Lotan-Pompan, O. Golani, G. Perry, M. Rokah, K. Bahar-Shany, E.A. Rozeman, C.U. Blank, A. Ronai, R. Shaoul, A. Amit, T. Dorfman, R. Kremer, Z.R. Cohen, S. Harnof, T. Siegal, E. Yehuda-Shnaidman, E.N. Gal-Yam, H. Shapira, N. Baldini, M.G. I. Langille, A. Ben-Nun, B. Kaufman, A. Nissan, T. Golan, M. Dadiani, K. Levanon, J. Bar, S. Yust-Katz, I. Barshack, D.S. Peeper, D.J. Raz, E. Segal, J.A. Wargo, J. Sandbank, N. Shental, R. Straussman, The human tumor microbiome is composed of tumor type–specific intracellular bacteria, Science 368 (6494) (2020) 973–980.

[5] X. Dong, P. Pan, D.-W. Zheng, P. Bao, X. Zeng, X.-Z. Zhang, Bioinorganic hybrid bacteriophage for modulation of intestinal microbiota to remodel tumor-immune microenvironment against colorectal cancer, Sci. Adv. 6 (20) (2020) eaba1590.

[6] G. El Tekle, W.S. Garrett, Bacteria in cancer initiation, promotion and progression, Nat. Rev. Cancer 23 (9) (2023) 600–618.

[7] N. Iida, A. Dzutsev, C.A. Stewart, L. Smith, N. Bouladoux, R.A. Weingarten, D. A. Molina, R. Salcedo, T. Back, S. Cramer, R.-M. Dai, H. Kiu, M. Cardone, S. Naik, A.K. Patri, E. Wang, F.M. Marincola, K.M. Frank, Y. Belkaid, G. Trinchieri, R. S. Goldszmid, Commensal bacteria control cancer response to therapy by modulating the tumor microenvironment, Science 342 (6161) (2013) 967–970.

[8] X. Kang, F. Bu, W. Feng, F. Liu, X. Yang, H. Li, Y. Yu, G. Li, H. Xiao, X. Wang, Dual-cascade responsive nanoparticles enhance pancreatic cancer therapy by eliminating tumor-resident intracellular bacteria, Adv. Mater. 34 (49) (2022) 2206765.

[9] O. Ciofu, C. Moser, P.Ø. Jensen, N. Høiby, Tolerance and resistance of microbial biofilms, Nat. Rev. Microbiol. 20 (10) (2022) 621–635.

[10] P.P. Kalelkar, M. Riddick, A.J. García, Biomaterial-based antimicrobial therapies for the treatment of bacterial infections, Nat. Rev. Mater. 7 (1) (2022) 39–54.

[11] W.E. Ruff, T.M. Greiling, M.A. Kriegel, Host-microbiota interactions in immune-mediated diseases, Nat. Rev. Microbiol. 18 (9) (2020) 521–538.

[12] S.R.S. Fishbein, B. Mahmud, G. Dantas, Antibiotic perturbations to the gut microbiome, Nat. Rev. Microbiol. 21 (12) (2023) 772–788.

[13] B.P. Willing, S.L. Russell, B.B. Finlay, Shifting the balance: antibiotic effects on host–microbiota mutualism, Nat. Rev. Microbiol. 9 (4) (2011) 233–243.

[14] C. Céire, M. Chris, L. Andrew, M. David, D.H. Alastair, Effect of antibiotic prescribing in primary care on antimicrobial resistance in individual patients: systematic review and meta-analysis, BMJ 340 (2010) c2096.

[15] S.J. Schrag, C. Peña, J. Fernández, J. Sánchez, V. Gómez, E. Pérez, J.M. Feris, R. E. Besser, Effect of short-course, high-dose amoxicillin therapy on resistant pneumococcal CarriageA randomized trial, JAMA 286 (1) (2001) 49–56.

[16] M. Wang, B. Rousseau, K. Qiu, G. Huang, Y. Zhang, H. Su, C. Le Bihan-Benjamin, I. Khati, O. Artz, M.B. Foote, Y.-Y. Cheng, K.-H. Lee, M.Z. Miao, Y. Sun, P.-J. Bousquet, M. Hilmi, E. Dumas, A.-S. Hamy, F. Reyal, L. Lin, P.M. Armistead, W. Song, A. Vargason, J.C. Arthur, Y. Liu, J. Guo, X. Zhou, J. Nguyen, Y. He, J.P. Y. Ting, A.C. Anselmo, L. Huang, Killing tumor-associated bacteria with a liposomal antibiotic generates neoantigens that induce anti-tumor immune responses, Nat. Biotechnol. (2023), https://doi.org/10.1038/s41587-023-01957-8.

[17] D.-W. Zheng, X. Dong, P. Pan, K.-W. Chen, J.-X. Fan, S.-X. Cheng, X.-Z. Zhang, Phage-guided modulation of the gut microbiota of mouse models of colorectal cancer augments their responses to chemotherapy, Nat. Biomed. Eng. 3 (9) (2019) 717–728.

[18] V. Biju, Chemical modifications and bioconjugate reactions of nanomaterials for sensing, imaging, drug delivery and therapy, Chem. Soc. Rev. 43 (3) (2014) 744–764.

[19] T. Wu, H. Wang, R. Tian, S. Guo, Y. Liao, J. Liu, B. Ding, A DNA origami-based bactericide for efficient healing of infected wounds, Angew. Chem. Int. Ed. 62 (46) (2023) e202311698.

[20] Y. Liu, L. Shi, L. Su, H.C. van der Mei, P.C. Jutte, Y. Ren, H.J. Busscher, Nanotechnology-based antimicrobials and delivery systems for biofilm-infection control, Chem. Soc. Rev. 48 (2) (2019) 428–446.

[21] P.W.K. Rothemund, Folding DNA to create nanoscale shapes and patterns, Nature 440 (7082) (2006) 297–302.

[22] S. Liu, Q. Jiang, X. Zhao, R. Zhao, Y. Wang, Y. Wang, J. Liu, Y. Shang, S. Zhao, T. Wu, Y. Zhang, G. Nie, B. Ding, A DNA nanodevice-based vaccine for cancer immunotherapy, Nat. Mater. 20 (3) (2021) 421–430.

[23] Q. Hu, H. Li, L. Wang, H. Gu, C. Fan, DNA Nanotechnology-enabled drug delivery systems, Chem. Rev. 119 (10) (2019) 6459–6506.

[24] H. Liang, X.-B. Zhang, Y. Lv, L. Gong, R. Wang, X. Zhu, R. Yang, W. Tan, Functional DNA-containing nanomaterials: cellular applications in biosensing, imaging, and targeted therapy, Acc. Chem. Res. 47 (6) (2014) 1891–1901.

[25] H. Pei, X. Zuo, D. Zhu, Q. Huang, C. Fan, Functional DNA nanostructures for theranostic applications, Acc. Chem. Res. 47 (2) (2014) 550–559.

[26] H. Majidzadeh, M. Araj-Khodaei, M. Ghaffari, M. Torbati, J. Ezzati Nazhad Dolatabadi, M.R. Hamblin, Nano-based delivery systems for berberine: a modern anti-cancer herbal medicine, Colloids Surf. B Biointerfaces 194 (2020) 111188.

[27] S. Khan, A. Hussain, F. Attar, S.H. Bloukh, Z. Edis, M. Sharifi, E. Balali, F. Nemati, H. Derakhshankhah, H.A. Zeinabad, F. Nabi, R.H. Khan, X. Hao, Y. Lin, L. Hua, T.L. M. ten Hagen, M. Falahati, Mitochondrial targeting nanodrugs self-assembled from 9-O-octadecyl substituted berberine derivative for cancer treatment by inducing mitochondrial apoptosis pathways, J. Contr. Release 294 (2019) 27–42.

[28] M. Yang, C. Yang, Y. Zhang, X. Yan, Y. Ma, Y. Zhang, Y. Cao, Q. Xu, K. Tu, M. Zhang, An oral pH-activated "nano-bomb" carrier combined with berberine by regulating gene silencing and gut microbiota for site-specific treatment of ulcerative colitis, Biomater. Sci. 10 (4) (2022) 1053–1067.

[29] T. Wu, Y. Fu, S. Guo, Y. Shi, Y. Zhang, Z. Fan, B. Yang, B. Ding, Y. Liao, Self-assembly multifunctional DNA tetrahedron for efficient elimination of antibiotic-resistant bacteria, Aggregate (2023) e402.

[30] G.S. Kumar, D. Debnath, A. Sen, M. Maiti, Thermodynamics of the interaction of berberine with DNA, Biochem. Pharmacol. 46 (9) (1993) 1665–1667.
[31] X. Tian, Y. Song, H. Dong, B. Ye, Interaction of anticancer herbal drug berberine with DNA immobilized on the glassy carbon electrode, Bioelectrochemistry 73 (2008) 18–22.
[32] J.C. Arthur, E. Perez-Chanona, M. Mühlbauer, S. Tomkovich, J.M. Uronis, T.-J. Fan, B.J. Campbell, T. Abujamel, B. Dogan, A.B. Rogers, J.M. Rhodes, A. Stintzi, K.W. Simpson, J.J. Hansen, T.O. Keku, A.A. Fodor, C. Jobin, Intestinal inflammation targets cancer-inducing activity of the microbiota, Science 338 (6103) (2012) 120–123.
[33] J. Song, C. Lin, X. Yang, Y. Xie, P. Hu, H. Li, W. Zhu, H. Hu, The microbial landscape of colorectal cancer, Nat. Rev. Microbiol. 22 (2024) 240–254.
[34] C. Urbaniak, G.B. Gloor, M. Brackstone, L. Scott, M. Tangney, G. Reid, The microbiota of breast tissue and its association with breast cancer, Appl. Environ. Microbiol. 82 (2016) 5039–5048.
[35] X.-L. Li, Y.-J. Hu, H. Wang, B.-Q. Yu, H.-L. Yue, Molecular spectroscopy evidence of berberine binding to DNA: comparative binding and thermodynamic profile of intercalation, Biomacromolecules 13 (2012) 873–880.